ACS OMEGA

Article

Cite This: ACS Omega 2018, 3, 13524−13529

http://pubs.acs.org/journal/acsodf

Probing Crystal Dislocations in a Micrometer-Thick GaN Film by Modern High-Voltage Electron Microscopy

Kazuhisa Sato*[,†,‡] and Hidehiro Yasuda[†,‡]

[†]Research Center for Ultra-High Voltage Electron Microscopy, Osaka University, 7-1 Mihogaoka, Ibaraki, Osaka 567-0047, Japan

[‡]Division of Materials and Manufacturing Science, Graduate School of Engineering, Osaka University, Suita, Osaka 565-0871, Japan

ABSTRACT: We report on extreme penetration power of relativistic electrons in a micrometer-thick gallium nitride epitaxial film and its application to probing threading dislocations, which were introduced during crystal growth. Maximum usable thickness of the specimen was quantitatively evaluated using high-voltage transmission electron microscopy (TEM) operating at 1 MV. The width of dislocation images was used as a measure for the evaluation of usable thickness. Superior maximum usable thickness was obtained in scanning transmission electron microscopy (STEM) than in TEM mode; the results were 6.9 μm for STEM and 4.4 μm for TEM. In STEM, dislocations can be imaged with an almost constant width of 15−20 nm in a wide thickness range 1−4 μm. The latest high-voltage STEM is thus useful for observing dislocations in micrometer-thick inorganic materials.

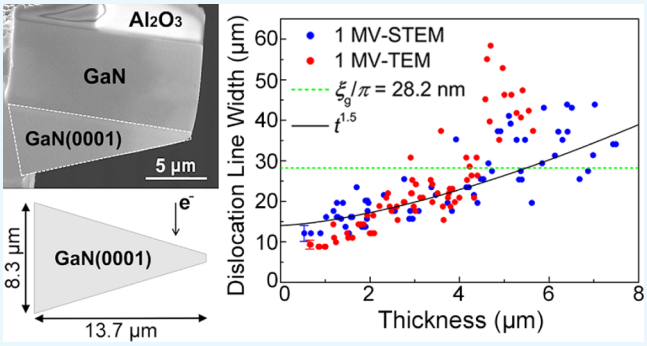

INTRODUCTION

Dislocations in a semiconductor crystal, such as gallium nitride (GaN), degrade its optical and electrical properties. The key to the development of high-performance light-emitting and electronic devices is the growth of highly complete crystals with a low dislocation density.[1] To detect and characterize lattice defects in a crystalline solid, transmission electron microscopy (TEM) is a powerful technique in respect of spatial resolution compared to other methods such as X-ray topography.[2] Imaging of dislocations by TEM is based on diffraction contrast, and the procedure has been established.[3] To visualize spatial distribution of dislocations, a novel approach was examined using electron tomography, which revealed three-dimensional dislocation networks in GaN.[4] However, electron transmittance limits the maximum usable (or observable) thickness of the specimen at most ∼0.3 μm in the case of conventional 200 kV TEM (this was examined by our preliminary study). The importance of observing sufficiently thick specimens that can be regarded as bulk was proved half a century ago using high-voltage electron microscopy (HVEM); namely, solid-state phenomena such as recrystallization, phase transition, and dynamic behaviors of crystal dislocations in metal foils thinner than a critical thickness differ from those observed in the bulk alloys.[5] In the years around 1970, considerable interest was focused on investigating the maximum usable thickness using HVEM.[6−11] However, the penetration of relativistic electrons depends on imaging conditions as well as materials,[12,13] and quantitative unified views regarding the maximum usable thickness have not been obtained. As mentioned above, the history of this topic is long over 50 years; however, recent interest in crystal defects and internal structures in semiconductor devices has drawn renewed attention to visualizing microstructures in an extremely thick specimen by HVEM.[14,15]

Recently, the authors reported that high-voltage (HV) scanning transmission electron microscopy (STEM) is capable of imaging dislocations in Si(110) crystals over 14 μm in thickness.[16] In principle, STEM has the benefit of being free from the effect of chromatic aberration since there is no imaging lens. Moreover, the technique is known to be less affected by the unfavorable diffraction contrast such as equal-thickness contour or bend contour (the word "unfavorable" is used here in a sense that aforementioned contours prevent clear-cut visualization of crystal defects such as dislocations).[17,18] This is due to the nature of STEM imaging using a converged electron probe. HV-STEM is hence the suitable imaging technique that can reveal the microstructures of a micrometer-order thick specimen in a nanometer-scale spatial resolution as well as a multiscale field of view.

In this study, we examined quantitative assessment of the maximum usable thickness of a GaN crystal with high-density threading dislocations (TDs) using HV-STEM and HV-TEM. TDs in GaN are mostly straight lines, and hence, they are expected to act as a good marker for discriminating transmittance of electrons. We show superior usable thickness in HV-STEM than in HV-TEM, and the obtained results are discussed.

Received: August 17, 2018
Accepted: October 9, 2018
Published: October 18, 2018

DOI: 10.1021/acsomega.8b02078
ACS Omega 2018, 3, 13524−13529

RESULTS

Figure 1a shows a secondary electron image of a wedge-shaped GaN crystal observed in an oblique direction. An isosceles triangle cross section is suitable for the systematic investigation of the usable thickness by HVEM. Cross section of the wedge-shaped specimen is schematically shown in Figure 1b. Electrons are incident on the wedge-shaped crystal from the direction indicated by an arrow, and also from the opposite direction for comparison. Thickness of the wedge-shaped specimen changes from 0.5 to 8.3 μm.

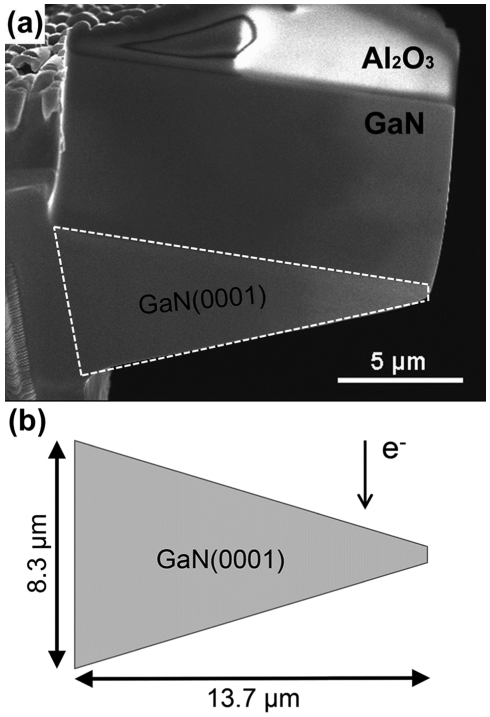

Figure 1. (a) SEM image of a wedge-shaped GaN crystal observed in an oblique direction. (b) Schematic illustration of the cross section of the wedge-shaped specimen.

Figure 2a shows a bright-field (BF) STEM image of the wedge-shaped GaN with high-density TDs. The specimen becomes thicker from the right (0.5 μm) to the left (2.5 μm) of the image. Appearance of the specimen and the selected area electron diffraction (SAED) pattern are shown in Figure 2b,c, respectively. We subjected a specimen to a two-beam condition by exciting the $\bar{1}100$ reflection. TDs are seen as lines almost parallel to $[0001]_{GaN}$ with dark contrast in a bright background, and the dislocation images become blurred as the thickness increases. Judging from the invisibility criterion for wurtzite GaN,[19,20] these TDs in GaN are almost either a-type (threading-edge) or a+c-type (threading-mixed). Note that c-type (threading-screw) TDs were identified by exciting 0002 reflection as well, while their number was a few. Then, the specimen was turned upside down and comparable observation was made (Figure 2d–f). In Figure 2d, the specimen becomes thicker from the left (0.5 μm) to the right (2.5 μm) of the image. It was found that the same dislocations were identified both in Figure 2d,a in the area with thickness at least less than 2.5 μm. Dislocation width was not affected by the observation direction to the specimen. It should also be noted that the width of dislocation images is independent of collection semiangle of the BF-STEM detector in the range of 4–25 mrad. As the collection semiangle increases, image intensity enhances, which leads to a brighter image contrast.

Figure 3 shows a composite BF-STEM image showing overall area of the wedge-shaped GaN specimen. The contrast

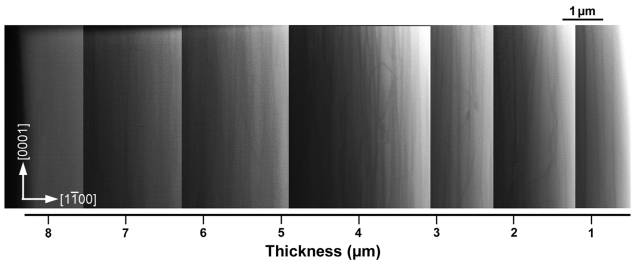

Figure 3. Composite BF-STEM image showing overall area of the wedge-shaped GaN specimen (g = $\bar{1}100$).

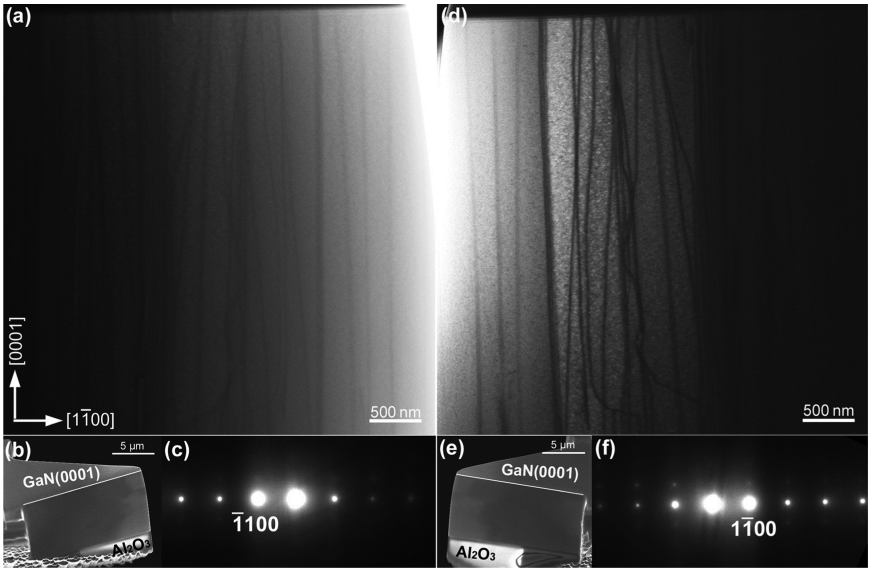

Figure 2. (a, d) BF-STEM images of the wedge-shaped GaN with high-density TDs, (b, e) appearance of the specimen, and (c, f) SAED patterns.

DOI: 10.1021/acsomega.8b02078
ACS Omega 2018, 3, 13524–13529

of each image was adjusted locally to show the dislocations clearly. The specimen becomes thicker from the right (0.5 μm) to the left (8.3 μm) of the image. Dislocation density was on the order of 10^{12} m^{-2} and was almost constant, regardless of the thickness, while apparent areal number density of TDs gradually increased as the thickness increased. On the basis of the analysis of areal number density of TDs, we found that overlapping of TDs in the observation direction is negligible, and hence, it little affects evaluation of the width of dislocation images. Dislocation images become blurred as the thickness increases. A notable feature is that it is possible to judge whether TDs exist even in the thick region with thickness around 7 μm. This is the direct evidence that 1 MeV electrons can transmit a 7 μm thick GaN crystal. More quantitative evaluation of the usable thickness is shown in Figure 6.

Figure 4 shows a composite BF-TEM image showing overall area of the wedge-shaped GaN, corresponding to the STEM

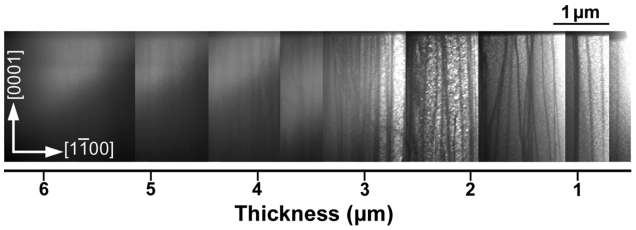

Figure 4. Composite BF-TEM image showing overall area of the wedge-shaped GaN specimen (g = $\bar{1}$100).

images shown in Figure 3. Dislocation images are almost invisible at thickness around 5 μm, indicating the superior usable thickness in STEM (i.e., Figure 3) than in TEM (i.e., Figure 4). Namely, usable thickness depends on the imaging mode, converged beam, or parallel beam, while the electron energy is the same in both cases (1 MeV).

Figure 5a,b compare BF-STEM and BF-TEM images of the same area with thickness of 0.8−2.2 μm. As can be seen, same dislocations are imaged in STEM and TEM modes, and this tendency was observed in the thickness range up to 4 μm. Thus, reciprocity of BF-STEM and BF-TEM can be confirmed qualitatively. Note that the dislocation image contrast in STEM is slightly sharper than that obtained in TEM. We found that annular dark-field (ADF) STEM at 1 MV was not useful for imaging dislocations in a thick specimen in respect of low detection efficiency due to weak intensity of an ADF-STEM signal. Namely, sufficient signal strength is mandatory for imaging microstructures in a micrometer-order thick specimen.

To quantitatively evaluate usable thickness, we measured width of dislocation images as a function of the specimen thickness. The width is defined as full width at half-maximum of the image intensity profile measured perpendicular to a dislocation line. Figure 6 shows the thickness dependence of the width of dislocation images measured from the STEM and TEM images. To avoid ambiguity regarding the visibility of dislocations, we introduced a criterion for the evaluation of usable thickness: theoretical dislocation width ξ_{hkl}/π (ξ_{hkl} stands for the extinction distance of the hkl reflection excited for imaging)[21] was employed as the criterion. Dashed line indicates the criterion $\xi_{\bar{1}100}/\pi$ = 28.2 nm ($\xi_{\bar{1}100}$ = 88.6 nm at 1 MV for GaN), and we judged that data points below this line are "observable". As seen, width of dislocation images increases

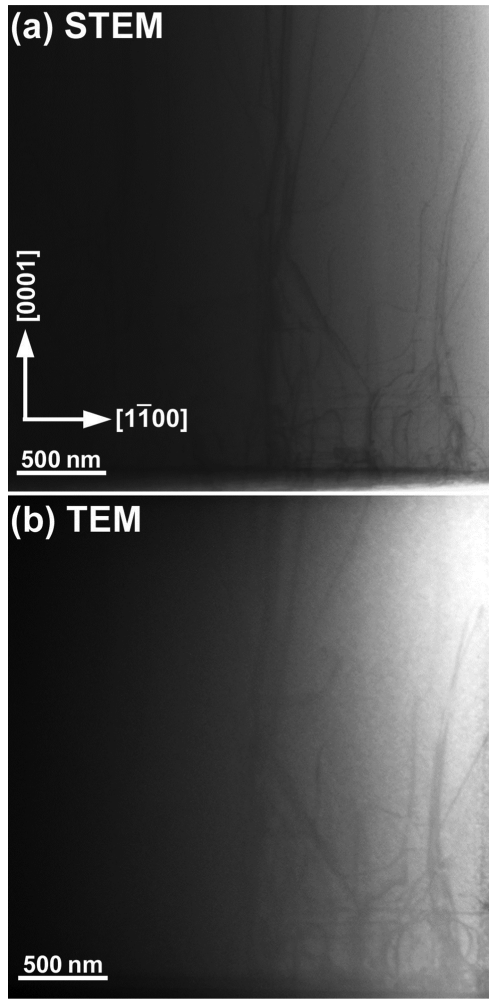

Figure 5. Comparison of (a) BF-STEM and (b) BF-TEM images obtained for the same area (g = $\bar{1}$100).

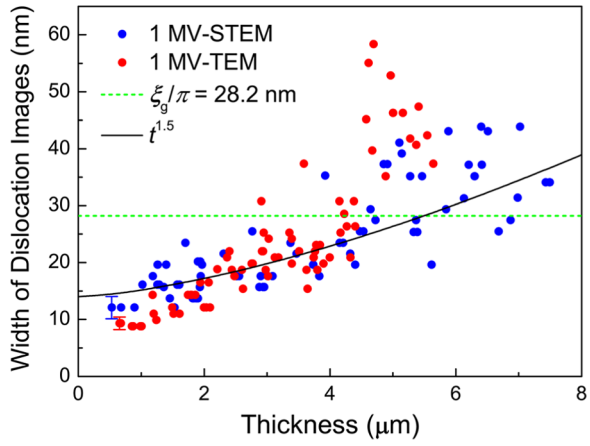

Figure 6. Thickness dependence of the width of the dislocation images measured from STEM and TEM images (g = $\bar{1}$100).

as the thickness increases. The obtained maximum usable thickness is 6.9 μm for BF-STEM and 4.4 μm for BF-TEM operating at 1 MV.

DISCUSSION

Focusing on the results of STEM, in the thickness range between 1 and 4 μm, we found that the width of dislocation

DOI: 10.1021/acsomega.8b02078
ACS Omega 2018, 3, 13524−13529

images shows weak thickness dependence and the values are distributed around 15−20 nm. This result may be related to the depth of focus of STEM. Let us consider a STEM probe with the convergence semiangle α and depth of focus Δz. Assuming the smallest converged STEM probe (approximately 1 nm at 1 MV in the present experimental setup), a depth of focus as short as 110 nm is derived using the following equation

$$\Delta z = 1.77\lambda/\alpha^2 \quad (1)$$

where λ denotes the wavelength of incident electrons.[22,23] However, same dislocations were observed irrespective of the beam incidence direction to the wedge-shaped specimen with the thickness less than 2.5 μm, which is 23 times longer than the short depth of focus estimated above (Figure 2). This result suggests that Δz defined by the eq 1 no longer serves as an indicator of the usable thickness. By contrast, assuming an object with a lateral length d, the extended depth of focus can be approximated as follows[16,22]

$$\Delta z_{ext} = d/\alpha \quad (2)$$

When d is equal to the width of dislocation image and by assigning the values of d = 20 nm and α = 3.75 mrad, Δz_{ext} = 5.3 μm is obtained. Namely, if we accept the blurring of the dislocation images at most 20 nm, a specimen with thickness up to approximately 5 μm can be imaged in focus using 1 MV STEM. This is a simple geometrical consideration but in good agreement with the experimental result shown above.

As the thickness increases more than 4 μm, the distribution of the width of dislocation images spreads rapidly (Figure 6). This is presumed to be due to possible lateral spread of the STEM probe (δ) proportional to $t^{3/2}$ (t denotes thickness of the specimen).[24] The solid curve shown in Figure 6 represents the fitted curve expressed as follows

$$\delta = 14 + 110\, t^{3/2} \quad (3)$$

As can be seen, beam broadening well represents the distribution of the data points for STEM.

Transmitted (T) and diffracted beam intensities (R) for 1 MV TEM were calculated by solving the Darwin−Howie−Whelan equations under a two-beam condition including absorption.[3] The T and R are expressed as follows[18]

$$T = \frac{e^{-\mu_0 t}}{2(1+w^2)}\left[(1+2w^2)\cosh\frac{\mu_g t}{\sqrt{1+w^2}} + 2w\sqrt{1+w^2}\sinh\frac{\mu_g t}{\sqrt{1+w^2}} + \cos\left(2\pi\frac{\sqrt{1+w^2}}{\xi_g}\right)t\right] \quad (4)$$

$$R = \frac{e^{-\mu_0 t}}{2(1+w^2)}\left[\cosh\frac{\mu_g t}{\sqrt{1+w^2}} - \cos\left(2\pi\frac{\sqrt{1+w^2}}{\xi_g}\right)t\right] \quad (5)$$

where s is the excitation error, ξ_0 is the extinction distance of the forward scattering, ξ_g is the extinction distance of the diffracted beam, ξ_0' and ξ_g' are attenuation terms of ξ_0 and ξ_g due to absorption, and t is the thickness that electrons propagate, with abbreviations $\mu_0 = 2\pi/\xi_0'$, $\mu_g = 2\pi/\xi_g'$, and $w = s\xi_g$. Figure 7a shows calculated thickness dependence of the T and R, assuming ξ_g = 88.6 nm (for $g = \bar{1}100_{GaN}$ at 1 MV), ξ_g'/ξ_g = 0.10, ξ_0'/ξ_g', and w = 0.40. Under these conditions, T reproduces the experimental result, i.e., T = 0.05 at t = 4.4 μm (=50ξ_g). Note that we assumed a criterion that the minimum of 5% of the transmitted beam should remain, and below which the image contrast is invisible. Intensity oscillations for both T and R are due to the equal-thickness fringes.

Figure 7b shows the parameter w dependence of T calculated for $t = 6\xi_g$, $12\xi_g$, and $50\xi_g$ at 1 MV. The peak

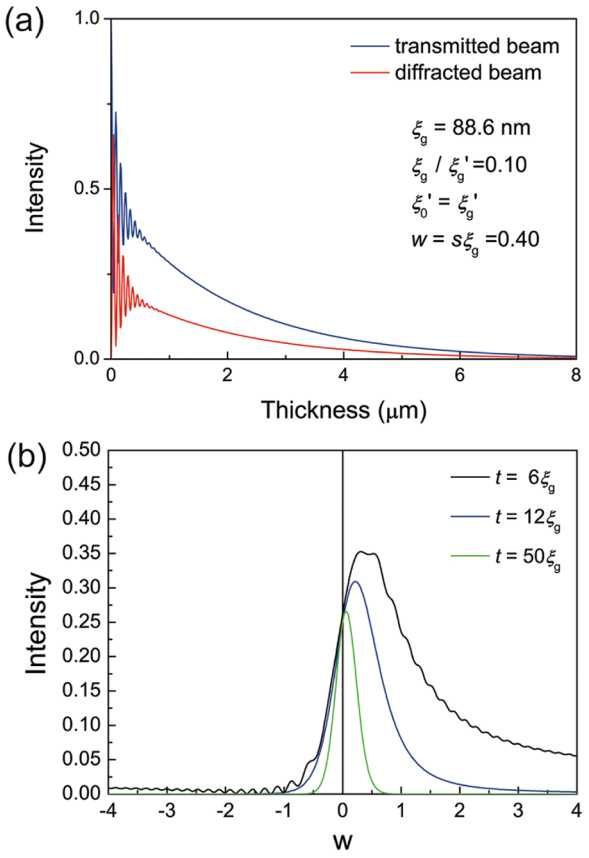

Figure 7. (a) Calculated thickness dependence of the transmitted beam (T) and the diffracted beam (R) at 1 MV. (b) Parameter w (=$s\xi_g$) dependence of T at 1 MV.

position shifts toward $w > 0$, especially for $t = 6\xi_g$ and $12\xi_g$. This represents the well-known fact that, for BF-TEM imaging in a two-beam condition, the best transmission can be obtained when s is slightly positive.[3] As the thickness increases, the peak position of the T shifts toward w = 0 and the peak height reduces. The calculation revealed that, to obtain the best transmission, fine adjustment of the parameter s, as possible as one can, is effective, depending on the specimen thickness. However, it should be noted that it is practically difficult to see diffracted beams when specimen thickness becomes fairly thick (e.g., $t = 50\xi_g$).

In this study, superior usable thickness in STEM to that in TEM was found, as shown in Figure 6. The similar tendency was obtained in our previous study on Si(110) wedge-shaped crystals,[16] where the effect of the spatial distribution of dislocations was not considered explicitly. By contrast, distribution of TDs in GaN can be regarded as statistically homogeneous; the results shown in Figure 6 are not affected by the spatial distribution of TDs.

DOI: 10.1021/acsomega.8b02078
ACS Omega 2018, 3, 13524−13529

In TEM observation, chromatic aberration arising from the postspecimen lens seriously degrades the resolution when observing a thick specimen. However, as already mentioned in the Introduction section, STEM requires no imaging lens for electrons transmitted through a specimen. Therefore, STEM is practically free from the effect of chromatic aberration, which may cause the superior usable thickness. From the viewpoint of chromatic aberration, the use of an energy filter (EF), which is based on electron energy-loss spectroscopy and hence inelastic scattering electrons can be either removed or selected, is also an effective solution. Using an EFTEM operating at 1.25 MV, Sadamatsu et al. reported a unique imaging technique incorporating inelastic scattering electrons; dislocations in a thick Si(001) over 10 μm have been imaged where zero-loss signal was absent.[25] Note that the maximum usable thickness of a wedge-shaped Si(110) crystal was 14.7 μm for 1 MV STEM.[16] Currently, HV-STEM and HV-EFTEM are useful methods for imaging microstructures in an extremely thick specimen, and a direct comparison between these two techniques regarding merits and demerits has not been examined yet, which will be clarified by investigations in the future.

CONCLUSIONS

We have studied the maximum usable thickness of the wedge-shaped GaN crystal in 1 MV STEM and 1 MV TEM using the width of dislocation images as a criterion for the quantitative evaluation. Superior usable thickness in STEM to that in TEM mode was demonstrated; the obtained results were 6.9 μm for STEM and 4.4 μm for TEM. In STEM mode, same dislocations were identified, regardless of the beam incidence direction to the wedge-shaped specimen when the thickness is less than 2.5 μm. Reciprocity of BF-STEM and BF-TEM was confirmed qualitatively as the same dislocations were imaged in STEM and TEM modes in the thickness range up to 4 μm. Intensity simulation reproduced the extreme penetration power of 1 MeV electrons. Fine adjustment of the excitation error is effective to obtain the best transmission.

EXPERIMENTAL PROCEDURES

TEM Specimen Preparation. To quantitatively evaluate the usable thickness by HV-STEM, we studied a hetero-epitaxial GaN film grown on α-Al_2O_3(0001). Wedge-shaped specimens were fabricated from the GaN film using a focused ion beam system. The specimen shapes were characterized using a scanning electron microscope (SEM) operating at 10 kV.

Characterization. Dislocations in a GaN film were observed using a JEOL JEM-1000EES operating at 1 MV equipped with a LaB_6 cathode. We subjected a specimen to a two-beam condition by exciting the $\bar{1}100$ or $1\bar{1}00$ reflection of wurtzite GaN. BF-TEM images were obtained using a 20 μm objective aperture with a semiangle of 2.8 mrad, and they were recorded using a 2k × 2k charge-coupled device camera (Gatan Orius SC200D) with an exposure time of 1−180 s. In the BF-STEM imaging, the beam convergence was set to a semiangle of 3.75 mrad using a 50 μm condenser aperture and the outer collection angle on the BF detector was set to 4−25 mrad. STEM images 1k × 1k in size were acquired with a dwell time of 256−1365 μs/pixel, depending on the specimen thickness.

AUTHOR INFORMATION

Corresponding Author

*E-mail: sato@uhvem.osaka-u.ac.jp.

ORCID

Kazuhisa Sato: 0000-0001-9078-2541

Hidehiro Yasuda: 0000-0002-9877-9803

Author Contributions

All authors contributed to the discussion and writing of the manuscript. The final version of the manuscript was approved by all authors.

Notes

The authors declare no competing financial interest.

ACKNOWLEDGMENTS

The authors wish to thank A. Ohsaki, Y. Agatsuma, S. Takakuwa, Dr S. Ohta, and M. Ohsaki of JEOL Ltd. for their support using the JEM-1000EES. K.S. acknowledges Professor Emeritus H. Mori of Osaka University for his invaluable comments. This study was partially supported by JSPS KAKENHI Grant Number JP17H02746.

REFERENCES

(1) Akasaki, I.; Amano, H. Breakthroughs in improving crystal quality of GaN and invention of the p-n junction blue-light-emitting diode. *Jpn. J. Appl. Phys.* **2006**, *45*, 9001−9010.

(2) Matsuhata, H.; Yamaguchi, H.; Ohno, T. Analysis of contrasts and identifications of Burgers vectors for basal-plane dislocations and threading edge dislocations in 4H-SiC crystals observed by monochromatic synchrotron X-ray topography in grazing-incidence Bragg-case geometry. *Philos. Mag.* **2012**, *92*, 4599−4617.

(3) Hirsch, P.; Howie, A.; Nicholson, R. B.; Pashley, D. W.; Whelan, M. J. *Electron Microscopy of Thin Crystals*, 2nd ed.; Krieger: Malabar, FL, 1977.

(4) Barnard, J. S.; Sharp, J.; Tong, J. R.; Midgley, P. A. Three-dimensional analysis of dislocation networks in GaN using weak-beam dark-field electron tomography. *Philos. Mag.* **2006**, *86*, 4901−4922.

(5) Fujita, H.; Kawasaki, Y.; Furubayashi, E.; Kajiwara, S.; Taoka, T. Metallurgical investigations with a 500 kV electron microscope. *Jpn. J. Appl. Phys.* **1967**, *6*, 214−230.

(6) Uyeda, R.; Nonomiya, M. The observation of thick specimens by high voltage electron microscopy. II. Experiments with molybdenite films at 50−1200 kV. *Jpn. J. Appl. Phys.* **1968**, *7*, 200−208.

(7) Hale, K. F.; Brown, M. H. Increase in penetration of electron microscope specimens at high voltages. *Nature* **1969**, *221*, 1232−1233.

(8) Fujita, H.; Tabata, T.; Yoshida, K.; Sumida, N.; Katagiri, S. Some applications of an ultra-high voltage electron microscope on materials science. *Jpn. J. Appl. Phys.* **1972**, *11*, 1522−1536.

(9) Fujita, H.; Tabata, T. Voltage dependence of the maximum observable thickness by electron microscopy up to 3 MV. *Jpn. J. Appl. Phys.* **1973**, *12*, 471−472.

(10) Thomas, G.; Lacaze, J. −C Transmission electron microscopy at 2.5 MeV. *J. Microsc.* **1973**, *97*, 301−308.

(11) Roucau, C.; Ayroles, R. Pénétration des électrons dans les corps de poids atomique élevé sous des tensions accélératrices ateignant 3000 kV cas de l'or et du tantale. *Philos. Mag.* **1975**, *31*, 387−404.

(12) Humphreys, C. J.; Thomas, L. E.; Lally, J. S.; Fisher, R. M. Maximizing the penetration in high voltage electron microscopy. *Philos. Mag.* **1971**, *23*, 87−114.

(13) Humphreys, C. J. The optimum voltage in very high voltage electron microscopy. *Philos. Mag.* **1972**, *25*, 1459−1472.

(14) Oshima, Y.; Nishi, R.; Asayama, K.; Arakawa, K.; Yoshida, K.; Sakata, T.; Taguchi, E.; Yasuda, H. Lorentzian-like image blur of gold nanoparticles on thick amorphous silicon films in ultra-high-voltage transmission electron microscopy. *Microscopy* **2013**, *62*, 521−531.

DOI: 10.1021/acsomega.8b02078
ACS Omega 2018, 3, 13524−13529

(15) Yamasaki, J.; Mutoh, M.; Ohta, S.; Yuasa, S.; Arai, S.; Sasaki, K.; Tanaka, N. Analysis of nonlinear intensity attenuation in bright-field TEM images for correct 3D reconstruction of the density in micron-sized materials. *Microscopy* **2014**, *63*, 345−355.
(16) Sato, K.; Yamashita, Y.; Yasuda, H.; Mori, H. Maximum usable thickness revisited: Imaging dislocations in Si by modern high-voltage scanning transmission electron microscopy. *Jpn. J. Appl. Phys.* **2017**, *56*, No. 100304.
(17) Humphreys, C. J. Fundamental concepts of STEM imaging. *Ultramicroscopy* **1981**, *7*, 7−12.
(18) Reimer, L. *Transmission Electron Microscopy*, 3rd ed.; Springer-Verlag: Berlin, Heidelberg, 1993.
(19) Phillips, P. J.; Brandes, M. C.; Mills, M. J.; De Graef, M. Diffraction contrast STEM of dislocations: Imaging and simulations. *Ultramicroscopy* **2011**, *111*, 1483−1487.
(20) Jones, K. A.; Batyrev, I. G. The structure of dislocations in (In, Al, Ga)N wurtzite films grown epitaxially on (0001) or (11$\bar{2}$2) GaN or AlN substrates. *J. Appl. Phys.* **2012**, *112*, No. 113507.
(21) Fultz, B.; Howe, J. M. *Transmission Electron Microscopy and Diffractometry of Materials*, 3rd ed.; Springer: Berlin, 2008.
(22) Nellist, P. D. The principles of STEM imaging. In *Scanning Transmission Electron Microscopy*; Pennycook, S. J., Nellist, P. D., Eds.; Springer: New York, 2011; Chapter 2.
(23) Kiguchi, T.; Yamaguchi, Y.; Tashiro, S.; Sato, K.; Konno, T. J. Effect of focal depth of HAADF-STEM imaging on the solute enriched layers in Mg alloys. *Mater. Trans.* **2015**, *56*, 1633−1638.
(24) *Energy-Filtering Transmission Electron Microscopy*; Reimer, L., Ed.; Springer-Verlag: Berlin, Heidelberg, 1995.
(25) Sadamatsu, S.; Tanaka, M.; Higashida, K.; Matsumura, S. Transmission electron microscopy of bulk specimens over 10 μm in thickness. *Ultramicroscopy* **2016**, *162*, 10−16.

DOI: 10.1021/acsomega.8b02078
ACS Omega 2018, 3, 13524−13529